Leptonic anomalous gauge couplings detection on electron positron colliders

Sheng-Zhi Zhao and Bin Zhang*

Department of Physics, Tsinghua University, Beijing, 100084, China, and Center for High Energy Physics,
Tsinghua University, Beijing, 100084, China

We studied the dimension-6 leptonic anomalous gauge couplings in the formulation of linearly realized gauge symmetry effective Lagrangian and investigated the constraints on these anomalous couplings from the existing experimental data, including LEP2 and W/Z boson decay. Some loose bounds of $O(0.1\text{--}10)$ TeV^{-2} on four relevant anomalous couplings are given by the Z factories. We studied the sensitivity of testing the leptonic anomalous couplings via the process $e^+e^- \rightarrow W^+W^-$ at future e^+e^- linear colliders. We discussed different sensitivities to anomalous couplings at polarized and unpolarized e^+e^- colliders, respectively, with 500 GeV and 1 TeV collision energy. Our results show that the 500 GeV International Linear Collider (ILC) can provide a test of the anomalous couplings, with the same relative uncertainty of cross section measurement, of $O(10^{-3}\text{--}10^{-2})$ TeV^{-2}, and a 1 TeV ILC can test the anomalous couplings of $O(10^{-4}\text{--}10^{-3})$ TeV^{-2}.

PACS numbers: 12.60.Cn, 13.66.Jn, 14.60.Cd, 14.70.−e

I. INTRODUCTION

The effective Lagrangian has long been an important model-independent approach for studying new physics beyond standard model (SM). It is customary to formulate new physics effects by linearly realizing the gauge symmetry [1,2]. After integrating out heavy degrees of freedom above the cutoff scale, the leading effects at low energies can be parametrized by the effective interactions. Reference [1] has systemically given all the gauge-invariant dimension-6 operators that can be constructed from the standard model fields. The coefficients of these anomalous operators, which are called ''anomalous couplings,'' reflect the strength of the new physics effects at low energies. There are already many theoretical studies that have suggested how to test the anomalous gauge couplings of the Higgs boson and gauge bosons in the literature for the LHC [3–7] and for the International Linear Collider (ILC) [8–10]. However, there has been much less effort put into understanding how to detect the anomalous gauge couplings of the fermions at colliders.

Since the discovery of neutrino oscillations in recent years [11], leptonic flavor physics, in particular, the neutrino mass and flavor mixing has become a hot topic in particle physics. Many theoretical models introduce heavy neutrinos or a fourth generation of leptons to explain the small neutrino masses [12]. In these models, the small neutrino masses are given by the seesaw mechanism. The seesaw mechanism generally requires heavy neutrino masses or very massive fourth generation leptons. It is very difficult to detect these particles directly at the LHC or other future colliders. However, the effects of those extra massive particles can be reflected in the anomalous couplings of leptons and gauge bosons in the low-energy effective Lagrangian. The measurement of the phenomenological effects of these leptonic anomalous gauge couplings on colliders will be useful in understanding the new physics beyond the standard model related with leptons and neutrinos. Furthermore, many new physical models of electroweak spontaneous symmetry breaking, such as little Higgs models [13], Higgsless models [14], and left-right symmetric gauge models [15], introduce mixing between extra gauge bosons and the ordinary gauge bosons of the standard model. As a result, there will be anomalous couplings, different from those of the standard model, between the fermions and the ordinary gauge bosons in those models. Detecting these leptonic anomalous gauge couplings on colliders can also test and verify these electroweak new physical models.

In this paper, we proposed the process $e^+e^- \rightarrow W^+W^-$ at the future electron-positron linear collider (ILC) to detect the anomalous couplings between the electron and the W, Z gauge bosons. This process is the simplest process at e^+e^- colliders, and both W and Z gauge couplings are involved in the process $e^+e^- \rightarrow W^+W^-$.

In the standard model the $e^+e^- \rightarrow W^+W^-$ process, there is a cancellation between the E^2 terms of different Feynman diagrams; therefore the total amplitude and cross section do not increase with collision energy. If anomalous couplings exist, the cancellation of energy power will be destroyed. Furthermore, the anomalous couplings will result in higher energy power dependence. Therefore, the existing low-energy electron-positron experiments give a very weak limit on the anomalous couplings, while the anomalous couplings are more likely to be detected at the future high-energy colliders.

---

*zb@mail.tsinghua.edu.cn

II. THE LEPTONIC ANOMALOUS GAUGE COUPLINGS IN EFFECTIVE LAGRANGIAN

To extend the structure of the SM in a model-independent approach, it is customary to formulate new physics effects by linearly realizing the gauge symmetry. After integrating out heavy degrees of freedom above the high scale Λ, the leading effects at low energies can be parametrized by the effective interactions

$$\mathcal{L}_{\text{eff}} = \sum_n \frac{f_n}{\Lambda^2} \mathcal{O}_n, \qquad (1)$$

where f_n's are dimensionless "anomalous couplings," and $\mathcal{O}_n$'s are the gauge-invariant dimension-6 operators, constructed from the SM fields. Leung, Love, and Rao [1] described all the dimension-6 $SU_c(3) \times SU_W(2) \times U(1)$ gauge-invariant operators. Of all these operators, there are six that involve leptonic gauge couplings and are CP even. They are

$$\mathcal{O}_7^{VF} = i\bar{L}\gamma_\mu W^{\mu\nu}\overleftrightarrow{D}_\nu L, \qquad \mathcal{O}_{11}^{VF} = i\bar{L}\gamma_\mu B^{\mu\nu}\overleftrightarrow{D}_\nu L,$$

$$\mathcal{O}_{13}^{VF} = i\bar{E}\gamma_\mu B^{\mu\nu}\overleftrightarrow{D}_\nu E, \qquad \mathcal{O}_{24}^{VF} = \bar{L}\gamma_\mu (D_\nu W^{\mu\nu})L,$$

$$\mathcal{O}_{26}^{VF} = \bar{L}\gamma_\mu \partial_\nu B^{\mu\nu}L, \qquad \mathcal{O}_{27}^{VF} = \bar{E}\gamma_\mu \partial_\nu B^{\mu\nu}E,$$

where L is left-hand $SU_W(2)$ lepton doublet and E is lepton right-hand singlet.

The Feynman rules for the vertices involving leptons and gauge bosons are listed in the Appendix. From these Feynman rules, we find that the operators $\mathcal{O}_7$ and $\mathcal{O}_{24}$ contribute to each of the vertices between leptons and gauge bosons in the process $e^+e^- \rightarrow W^+W^-$. These two operators even provide an additional four-line $l^+l^-W^+W^-$ vertex. However, other operators $\mathcal{O}_{11}$, $\mathcal{O}_{13}$, $\mathcal{O}_{26}$, and $\mathcal{O}_{27}$ only affect the neutral current vertices. Therefore, the process $e^+e^- \rightarrow W^+W^-$ is much more sensitive to operators $\mathcal{O}_7$ and $\mathcal{O}_{24}$ than others. The two operators $\mathcal{O}_{11}$ and $\mathcal{O}_{13}$ are only involved in the initial electron-positron fusion vertices in the S channel diagrams, and the three momentums of the neutral current vertices are parallel. The construction of the two operators' Feynman rules determine that their contributions are zero when all three momentums are parallel, as we can see from the Feynman rule (b) in the Appendix.

III. THE CONSTRAINTS FROM LEP2 AND W/Z DECAY

The measurement of the total cross section of W pair production on experiment LEP2 [16] can give some limits on the anomalous coupling constants. However, because the collision energy is just beyond the W pair threshold, the W bosons produced at LEP2 typically have low momentum. The effects of dimension-6 operators are very small. In other words, the constraints from LEP2 are very weak.

In this work, we only calculate the cross section of $e^+e^- \rightarrow W^+W^-$ at tree level and figure out the relative deviations from the standard model caused by various anomalous couplings. We make the reasonable assumption that the relative deviation will not be changed significantly by radiative correction and detector simulation. The LEP2 experimental measurement of the cross section for the process $e^+e^- \rightarrow W^+W^-$ is highly consistent with theoretical calculation. The systematic uncertainty of experimental measurement can conversely give constraints on the anomalous couplings. The relative uncertainty of cross section measurement is about $\pm 2\%$ at LEP2 [16]. Here, we conservatively enlarged the experimental uncertainty and theoretical uncertainty to $\pm 5\%$, and any cross section deviations beyond $\pm 5\%$ caused by anomalous couplings can be detected at colliders. We also suppose the same uncertainty for future linear colliders.

In accordance with the experiment, we let the final W bosons decay to fermions and impose the following acceptance cuts on final fermions:

$$|\eta| < 3, \qquad p_T > 10 \text{ GeV}.$$

After the cuts, the standard model detectable W pair product cross section is 17.7 pb at tree level. Figure 1 plots the relative deviations caused, respectively, by different anomalous coupling constants.

According to the experimental relative uncertainty $\pm 5\%$, the LEP2 measurement on the cross section can provide the limits on anomalous couplings:

$$-2.7 \text{ TeV}^{-2} < f_7/\Lambda^2 < 2.7 \text{ TeV}^{-2},$$

$$-9.8 \text{ TeV}^{-2} < f_{24}/\Lambda^2 < 1.8 \text{ TeV}^{-2},$$

$$-11 \text{ TeV}^{-2} < f_{26}/\Lambda^2 < 33 \text{ TeV}^{-2},$$

$$-13 \text{ TeV}^{-2} < f_{27}/\Lambda^2 < 30 \text{ TeV}^{-2}.$$

The bounds on the four relevant anomalous couplings from the LEP2 experiment are very loose, because the outgoing W bosons do not obtain large momentums compared to their mass. However, the dimension-6 anomalous couplings should have been enhanced by large momentums.

The measurements of the W boson decay width and the leptonic branching ratio have very high accuracy, and they also can provide limits on anomalous couplings. However only one anomalous coupling f_{24} can change the W decay amplitude. In Fig. 2 we have plotted the numerical calculated relative deviations of the W boson leptonic decay partial width caused by the anomalous coupling constants f_{24}. The f_{24} anomalous coupling can increase or decrease the leptonic decay partial width because of the interference with the standard vertex.

We can also give the analytical form of the relative deviations of the W boson leptonic decay partial width
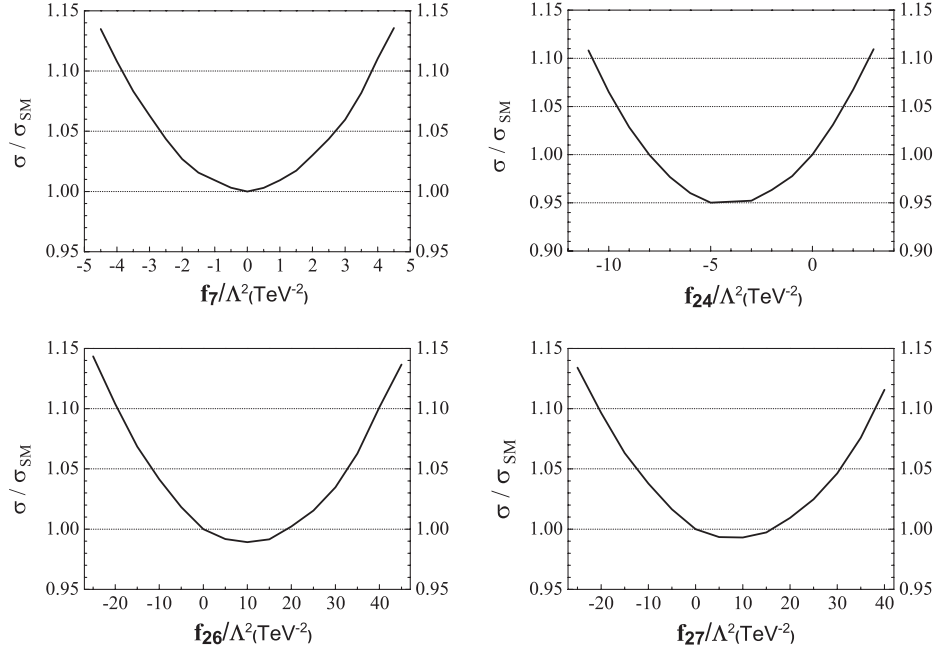
FIG. 1. The relative deviations of $e^+e^- \rightarrow W^+W^-$ cross section on LEP2 caused by different anomalous coupling constants.

caused by the anomalous coupling constants f_{24}. The $W\ell\nu$ vertex with anomalous coupling is $\frac{i\gamma^\mu}{\sqrt{2}}\frac{e}{s}P_L + \frac{i}{\Lambda^2}[\not{k}_1 k_1^\mu - k_1^2\gamma^\mu](-\frac{\sqrt{2}}{2}f_{24})P_L$ as listed in the Appendix in (c), where k_1 is the W's momentum. Because the W boson is on-shell in the decay process, the vertex is simplified to $\frac{i\gamma^\mu}{\sqrt{2}}(\frac{e}{s} + \frac{M_W^2}{\Lambda^2}f_{24})P_L$. The anomalous coupling f_{24} can change the SM W boson leptonic decay partial width $\Gamma_{sm} \propto (\frac{e}{s})^2$ to $\Gamma(f_{24}) \propto (\frac{e}{s} + \frac{M_W^2}{\Lambda^2}f_{24})^2$. When the anomalous coupling is small, the relative deviations of the W boson leptonic decay partial width become

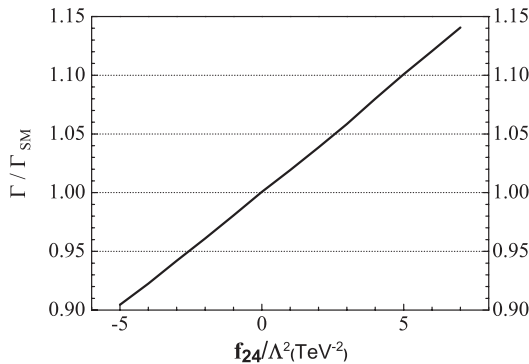$$\frac{\Delta\Gamma(f_{24})}{\Gamma_{sm}} \approx \frac{2M_W^2 s}{e}\frac{f_{24}}{\Lambda^2}.$$

FIG. 2. The relative deviations of W boson leptonic decay partial width caused by the anomalous coupling constants f_{24}.

It is the same as the numerical calculation result plotted in Fig. 2.

The experimental relative uncertainties of the W boson decay width and the leptonic branching ratio are very small, both within $\pm 2\%$ [17], so the relative uncertainty of the leptonic decay partial width is also within $\pm 2\%$. Therefore, the measurement of the W boson decay can provide a more stringent limit on anomalous coupling f_{24}:

$$-1.03 \text{ TeV}^{-2} < f_{24}/\Lambda^2 < 1.03 \text{ TeV}^{-2}.$$

The measurement of the Z boson leptonic partial decay width has much higher accuracy than that of the W boson decay, so it can provide more stringent limits on anomalous couplings. There are three anomalous couplings f_{24}, f_{26}, and f_{27}, which can affect the Z decay amplitude. The three anomalous couplings change the $Z\ell\ell$ vertex to be $i\gamma^\mu(\frac{e(2s^2-1)}{2cs}P_L + \frac{es}{c}P_R) + \frac{i}{\Lambda^2}[\not{k}_1 k_1^\mu - k_1^2\gamma^\mu](\frac{c}{2}f_{24}P_L + sf_{26}P_L + sf_{27}P_R)$ as listed in the Appendix, where k_1 is the Z's momentum. When the Z boson is on-shell in the decay process, the vertex is simplified to

$$i\gamma^\mu\left(\frac{e(2s^2-1)}{2cs} - \frac{M_Z^2}{\Lambda^2}\left(\frac{c}{2}f_{24} + sf_{26}\right)\right)P_L$$
$$+ i\gamma^\mu\left(\frac{es}{c} - \frac{M_Z^2}{\Lambda^2}sf_{27}\right)P_R.$$

While the anomalous couplings are small, the relative deviations of the Z boson leptonic decay partial width become

$$\frac{\Delta\Gamma}{\Gamma_{sm}} \approx \frac{\frac{e(2s^2-1)}{2s}\frac{M_Z^2}{\Lambda^2}(f_{24}+\frac{s}{2c}f_{26}) + 2\frac{es}{c}\frac{M_Z^2}{\Lambda^2}sf_{27}}{(\frac{e(2s^2-1)}{2cs})^2 + (\frac{es}{c})^2}.$$

The experimental relative uncertainty of the Z boson leptonic partial decay width is very small, within $\pm 0.2\%$ [17]. Therefore, the measurement of the Z boson decay can provide much more stringent limits on anomalous couplings:

$$-0.1 \text{ TeV}^{-2} < f_{24}/\Lambda^2 < 0.1 \text{ TeV}^{-2},$$

$$-0.09 \text{ TeV}^{-2} < f_{26}/\Lambda^2 < 0.09 \text{ TeV}^{-2},$$

$$-0.11 \text{ TeV}^{-2} < f_{27}/\Lambda^2 < 0.11 \text{ TeV}^{-2}.$$

The measurements of the Z effective axial-vector couplings g_A to charged leptons are also the most accurate experiments at the Z factories together with the Z boson decay width. We may also analyze the constraint from the high-precision measurements of g_A. Three anomalous couplings can provide the extra axial-vector coupling, and we define the anomalous axial-vector coupling as $f_A = (f_{24} + \frac{2s}{c}f_{26} - \frac{2s}{c}f_{27})$. The axial-vector current vertex becomes $i\gamma^\mu\gamma^5(-\frac{e}{2cs}g_A + \frac{M_Z^2}{\Lambda^2}\frac{c}{4}f_A)$ when Z is on-shell, where g_A is the effective axial-vector coupling of the Z boson to charged leptons with $g_A = 0.5$ in the standard model. Meanwhile the high-precision measurements of g_A can give a stringent bound on the anomalous axial-vector coupling f_A. The high-precision g_A magnitude is derived from measurements of the Z line shape and the

forward-backward lepton asymmetries as a function of energy around the Z mass; the measurements have the collision energy close to the Z mass, and the Z bosons are almost on-shell. Hence the relative deviation of g_A caused by the axial-vector coupling f_A is

$$\frac{\Delta g_A}{g_A} = -\frac{M_Z^2 c^2 s}{e}\frac{f_A}{\Lambda^2}. \tag{2}$$

The experimental relative uncertainty on g_A is very small, within $\pm 0.1\%$ [17]. To limit the deviation of g_A to within $\pm 0.1\%$, a very stringent limit on anomalous couplings combination f_A, we have

$$-0.1 \text{ TeV}^{-2} < f_A/\Lambda^2 < 0.1 \text{ TeV}^{-2}.$$

IV. THE DETECTION OF LEPTONIC ANOMALOUS GAUGE COUPLINGS AT ILC

The anomalous couplings bring high-energy power dependence to the $e^+e^- \to W^+W^-$ cross section. The higher the collision energy, the greater the deviation caused by anomalous couplings. We have considered the relative deviations caused by different anomalous couplings at the future ILC with the collision energy $\sqrt{s_{ee}} = 500$ GeV in Fig. 3, and at $\sqrt{s_{ee}} = 1$ TeV ILC in Fig. 4. The total cross section decreases as the collision energy increases and is concentrated in the forward region. The quarks or leptons produced in the decays of the energetic W bosons
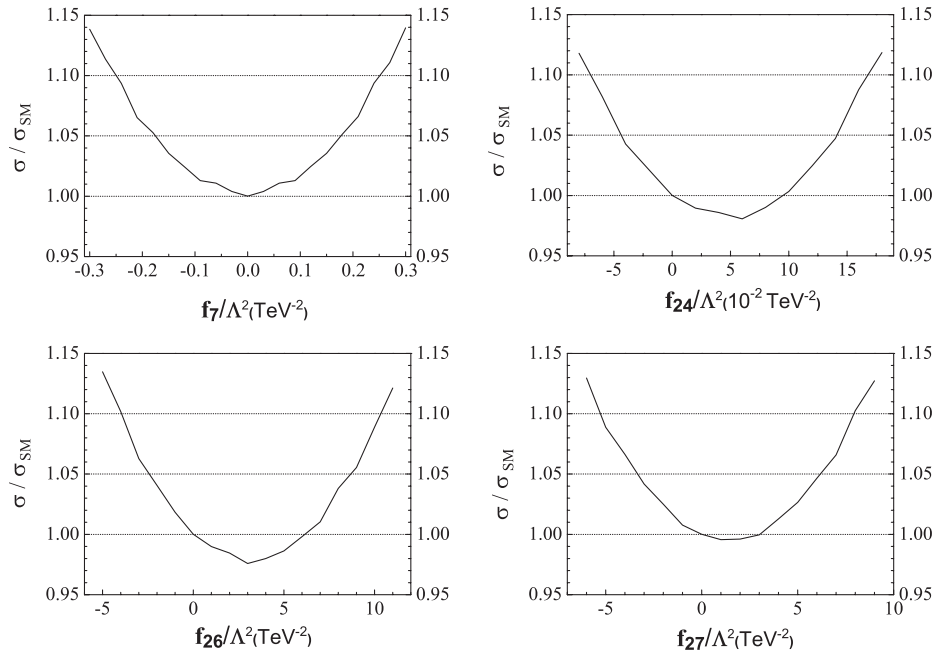

FIG. 3.   The relative deviations of $e^+e^- \to W^+W^-$ cross section on 500 GeV ILC caused by various anomalous couplings.
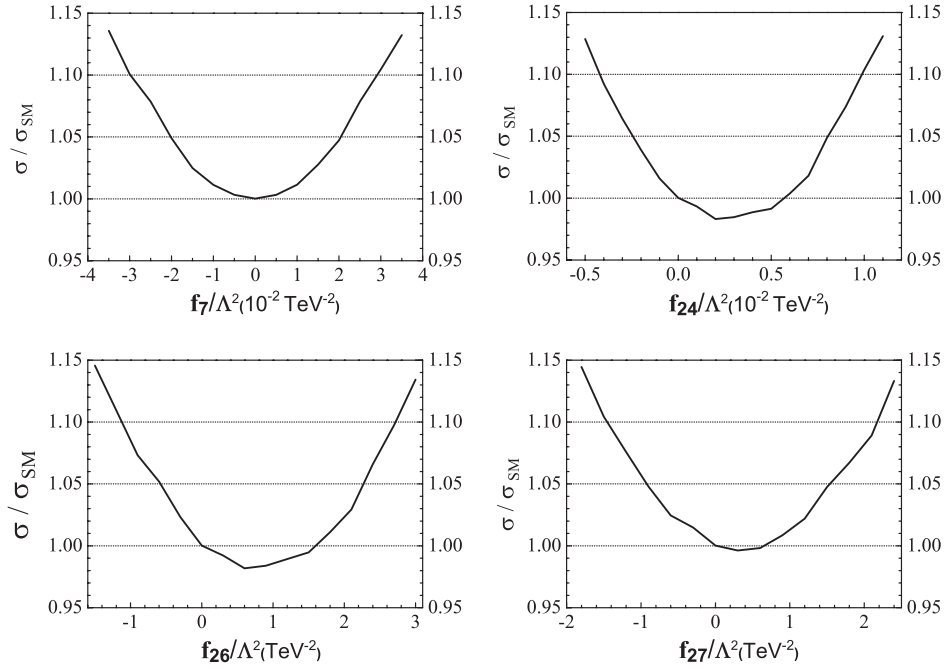
FIG. 4. The relative deviations of $e^+e^- \rightarrow W^+W^-$ cross section on 1 TeV ILC caused by various anomalous couplings.

follow the forward alignment such that the basic acceptance cuts reduce the cross section more severely. The standard model total cross section after basic cuts is about 5.68 pb as $\sqrt{s_{ee}} = 500$ GeV and 1.42 pb as $\sqrt{s_{ee}} = 1$ TeV. However, the large luminosity of ILC will still provide sufficient events to analyze the effect of the anomalous couplings. We also suppose the ILC can reach the same experimental relative uncertainty on the cross section as LEP2 and the constraint on the detection ability still comes from the experimental uncertainty.

The detection ability of high-energy ILC is much better than LEP2. If we also suppose that the same experimental relative uncertainty of the cross section on ILC is $\pm 5\%$, the detection sensitivities of the anomalous coupling constants of $\sqrt{s_{ee}} = 500$ GeV ILC are

$$-0.18 \text{ TeV}^{-2} < f_7/\Lambda^2 < 0.18 \text{ TeV}^{-2},$$
$$-0.042 \text{ TeV}^{-2} < f_{24}/\Lambda^2 < 0.14 \text{ TeV}^{-2},$$
$$-2.3 \text{ TeV}^{-2} < f_{26}/\Lambda^2 < 8.6 \text{ TeV}^{-2},$$
$$-3.3 \text{ TeV}^{-2} < f_{27}/\Lambda^2 < 6.2 \text{ TeV}^{-2}.$$

And, the detection sensitivities of the anomalous coupling constants of $\sqrt{s_{ee}} = 1000$ GeV ILC are

$$-2.0 \times 10^{-2} \text{ TeV}^{-2} < f_7/\Lambda^2 < 2.0 \times 10^{-2} \text{ TeV}^{-2},$$
$$-2.5 \times 10^{-3} \text{ TeV}^{-2} < f_{24}/\Lambda^2 < 8.0 \times 10^{-3} \text{ TeV}^{-2},$$
$$-0.6 \text{ TeV}^{-2} < f_{26}/\Lambda^2 < 2.3 \text{ TeV}^{-2},$$
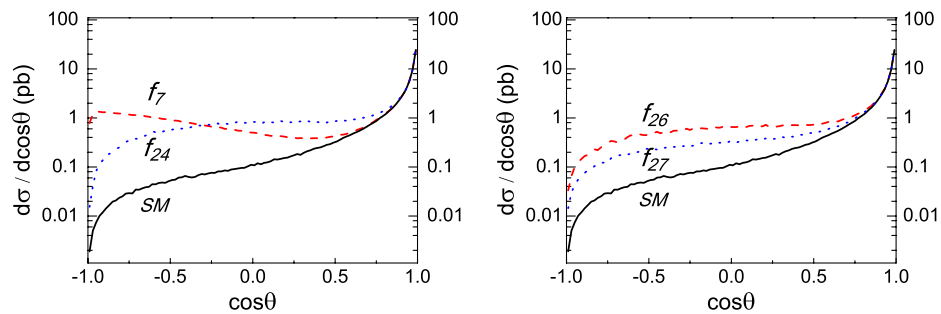$$-0.9 \text{ TeV}^{-2} < f_{27}/\Lambda^2 < 1.5 \text{ TeV}^{-2}.$$

FIG. 5 (color online). The W boson outgoing angle distribution at 1 TeV ILC. The solid curve is the SM distribution, and the dashed and dotted curves are the distributions, respectively, with $f_7/\Lambda^2 = 8 \times 10^{-2} \text{ TeV}^{-2}$; $f_{24}/\Lambda^2 = 2 \times 10^{-2} \text{ TeV}^{-2}$; $f_{26}/\Lambda^2 = 6 \text{ TeV}^{-2}$; $f_{27}/\Lambda^2 = 3 \text{ TeV}^{-2}$.
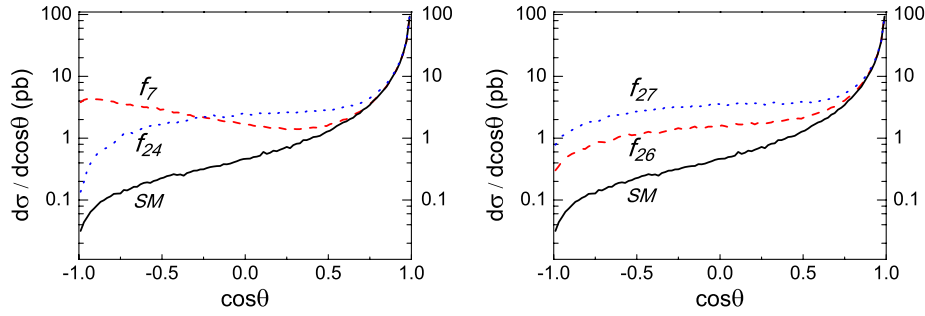
FIG. 6 (color online). The W boson outgoing angle distribution at 500 GeV ILC. The solid curve is the SM distribution, and the dashed and dotted curves are the distributions, respectively, with $f_7/\Lambda^2 = 0.6$ TeV^{-2}; $f_{24}/\Lambda^2 = 0.3$ TeV^{-2}; $f_{26}/\Lambda^2 = 15$ TeV^{-2}; $f_{27}/\Lambda^2 = 20$ TeV^{-2}.

The detection sensitivities at ILC are increased by 1–2 orders of magnitude more than at the LEP2.

V. THE W BOSON ANGULAR DISTRIBUTION OF THE ANOMALOUS SIGNATURE

We also analyzed the distribution of the cross section in order to find the sensitive region of the anomalous coupling. The W outgoing angle is the unique kinematic parameter in the process $e^+e^- \rightarrow W^+W^-$ at the energy determined e^+e^- colliders, and the W angle can be reconstructed from the W decay final states on ILC. Therefore, we analyzed the angular distribution of the final state W particle and compared the distribution differences between anomalous couplings and the standard model.

Figures 5 and 6 show the differences on W^- boson outgoing angle distribution, where θ_{W^-} is the W^- production angle with respect to the direction of the incoming electrons. The distribution of the W^+ production angle with respect to the direction of the incoming positrons θ_{W^+} is the same for the charge symmetry. To give the distribution of the angle of the W^- or W^+ bosons, it is necessary to distinguish the sign of the W charge in the experiment. Therefore, only the semileptonic decay of the W pairs can be considered, $e^+e^- \rightarrow W^+W^- \rightarrow qq\ell\nu$, where the final leptons only include $\mu^\pm$ and $e^\pm$. So the semileptonic decay branching ratio is $66\% \times 21\% \times 2 = 27.7\%$. For the standard model, the cross section is mainly

distributed in the forward region where $\cos\theta_{W^\pm}$ is close to 1, because the T channel neutrino exchange diagram is dominant. The anomalous couplings' relative effect to the cross section is much larger in the small $\cos\theta_{W^\pm}$ area, but the partial cross section in this region is very small as shown in the figures. The trend becomes more obvious with the higher collision energy. The standard model cross section within $\cos\theta_{W^\pm} < 0.75$ is 0.28 pb at a 1 TeV ILC and decreases to 0.146(0.053) pb within $\cos\theta < 0.5(0)$. If the integrated luminosity of ILC is large enough (for example, $\int \mathcal{L} \geq 46.2$ fb^{-1}), one can apply a W angle cut (for instance, $\cos\theta < 0.75$) to improve the detection sensitivity. In this case, the standard model will provide more than $\sigma_{SM}(\cos\theta < 0.75) \times Br \times \int \mathcal{L} = 3600$ events, and the significance of 5% relative deviation caused by anomalous couplings will be greater than 3σ (the significance defined as $N_s/\sqrt{N_B}$). If the integrated luminosity becomes greater, we can take a more stringent W angle cut. The cut $\cos\theta < 0.5$ can be applied and still keep 3σ significance when $\int \mathcal{L} \geq 90.2$ fb^{-1} and the cut $\cos\theta < 0$ can be applied if $\int \mathcal{L} \geq 245$ fb^{-1}, as listed in Table I. The total cross section at a 500 GeV ILC is larger than at a 1 TeV ILC, and the effect of a W outgoing angle cut at a 500 GeV ILC is not as obvious as at a 1 TeV ILC, so the requirement of the integrated luminosity is much smaller. For the process at the 200 GeV LEP2, as shown in Fig. 7, the outgoing W bosons are not very forward because the W momentum is small compared to its rest mass. The W outgoing angle cut

TABLE I. The cross sections after different W angle cuts on $\sqrt{s_{ee}} = 500$ GeV and 1 TeV ILC and the required integrated luminosity for 5% relative deviation to keep 3σ significance.

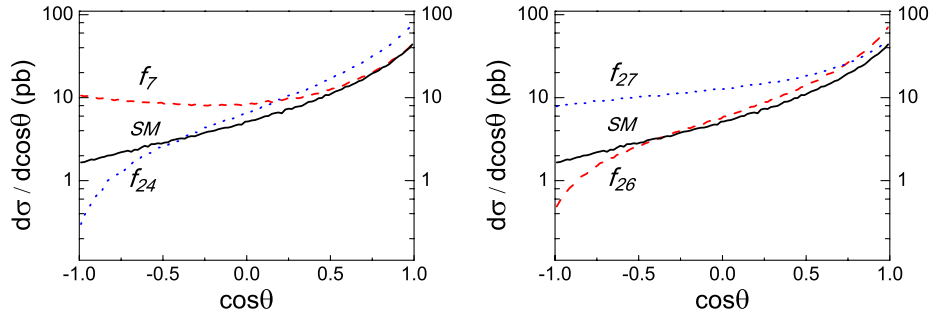| $\cos\theta$ cut	σ (500 GeV)	Required $\int \mathcal{L}$	σ (1 TeV)	Required $\int \mathcal{L}$
None	5.68 pb	0.63 fb^{-1}	1.42 pb	2.5 fb^{-1}
$\cos\theta < 0.75$	1.14 pb × 27.7%	11.2 fb^{-1}	0.28 pb × 27.7%	46.2 fb^{-1}
$\cos\theta < 0.5$	0.61 pb × 27.7%	21.3 fb^{-1}	0.146 pb × 27.7%	90.2 fb^{-1}
$\cos\theta < 0$	0.23 pb × 27.7%	56.3 fb^{-1}	0.053 pb × 27.7%	245 fb^{-1}

FIG. 7 (color online).   The W boson outgoing angle distribution at 200 GeV LEP2. The solid curve is the SM distribution, and the dashed and dotted curves are the distributions, respectively, with $f_7/\Lambda^2 = 8$ TeV^{-2}; $f_{24}/\Lambda^2 = 9$ TeV^{-2}; $f_{26}/\Lambda^2 = 60$ TeV^{-2}; $f_{27}/\Lambda^2 = 90$ TeV^{-2}.
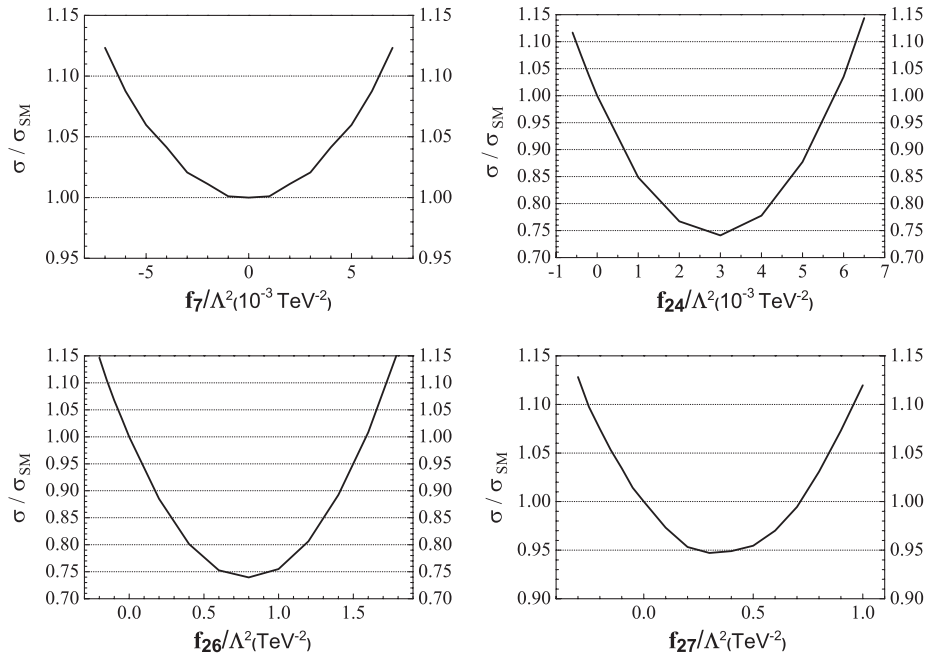

FIG. 8.   The relative deviations of $e^+ e^- \rightarrow W^+ W^-$ cross section on 500 GeV ILC caused by different anomalous coupling constants.

at the 200 GeV LEP2 is almost not helpful to improve the detection limits of anomalous couplings, except a little improvement on f_7.

The more stringent W angle cut can give the better sensitivity on anomalous couplings detection, while the remaining cross section is lower and required luminosity becomes greater, as listed in Table. I. The relative deviations caused by various anomalous couplings after the W outgoing angle cut $\cos\theta < 0$ are shown in Fig. 8 as an example, where the collision energy $\sqrt{s_{ee}} = 1$ TeV.

TABLE II.   The detection limits of the anomalous coupling constants on $\sqrt{s_{ee}} = 500$ GeV ILC with different W outgoing angle cuts.

$\cos\theta$ cut	$f_7/\Lambda^2(10^{-2}$ TeV$^{-2})$	$f_{24}/\Lambda^2(10^{-2}$ TeV$^{-2})$	$f_{26}/\Lambda^2(10^{-1}$ TeV$^{-2})$	$f_{27}/\Lambda^2($TeV$^{-2})$
None	-18–18	-4.2–14	-23–86	-3.3–6.2
$\cos\theta < 0.75$	-8–8	-1.1–1.5	-6.4–8.1	-1.2–4.0
$\cos\theta < 0.5$	-5.9–5.9	-0.67–0.95	-4.1–4.9	-0.76–3.6
$\cos\theta < 0$	-3.8–3.8	-0.44–0.5	-2.5–2.8	-0.49–0.99

TABLE III. The detection limits of the anomalous coupling constants on $\sqrt{s_{ee}} = 1$ TeV ILC with different W outgoing angle cuts.

$\cos\theta$ cut	$f_7/\Lambda^2(10^{-3}$ TeV$^{-2})$	$f_{24}/\Lambda^2(10^{-4}$ TeV$^{-2})$	$f_{26}/\Lambda^2(10^{-1}$ TeV$^{-2})$	$f_{27}/\Lambda^2(10^{-1}$ TeV$^{-2})$
None	−20–20	−25–80	−6–23	−9–15
$\cos\theta < 0.75$	−9.5–9.5	−6.7–10	−1.9–2.3	−3.3–10
$\cos\theta < 0.5$	−6.5–6.5	−4.2–5.0	−1.1–1.4	−2.0–9.2
$\cos\theta < 0$	−4.6–4.6	−2.8–2.9	−0.75–0.78	−1.4–2.5

From Fig. 8, we can see that some specific anomalous coupling values can reduce the final cross section beyond 5%. The cross section decreases because of the interference between the anomalous couplings and the standard model couplings.

Tables II and III give the detection limits of the $\sqrt{s_{ee}} = 500$ GeV and 1 TeV ILC, respectively. Within the limits, the relative deviations of the cross section caused by anomalous couplings are less than $\pm 5\%$, which cannot be detected at the ILC. If any listed anomalous couplings go beyond their relevant bounds, the ILC can survey the deviation from the standard model. The more stringent a W angle cut applied, the better detection sensitivity ILC can provide. We can see from Table III, after a W angle cut, the ILC detection sensitivity is increased by 3–4 orders of magnitude more than the LEP2.

VI. THE POLARIZATION SCHEME

We also considered ILC with the polarization scheme. Both in standard model and in anomalous couplings, the W boson only couples to left-handed leptons. If the initial electrons are right-handed polarized, they only couple to neutral gauge boson Z and γ. So the process $e_L^+ e_R^- \rightarrow W^+W^-$ only has Z/γ S channel Feynman diagrams. Therefore the ILC with polarization scheme will be very useful to detect the anomalous coupling between the lepton and Z boson. The standard model's right-handed polarized cross section is 107 fb with $\sqrt{s_{ee}} = 500$ GeV and 22.2 fb with $\sqrt{s_{ee}} = 1$ TeV. The cross section is still large enough

to analyze $\pm 5\%$ relative deviation with a certain integrated luminosity.

It is different from the unpolarized ILC scheme; the process with right-handed polarized electrons is very sensitive to the coefficient f_{27}, which only appears in the anomalous coupling between the lepton and Z boson and is not sensitive in the unpolarized $e^+e^- \rightarrow W^+W^-$ process. In the polarized S channel process, the anomalous coupling f_{27} can interfere with the standard model coupling, and the relative deviations of the cross section are shown in Fig. 9.

If we also suppose the same experimental relative uncertainty of the cross section at the polarized ILC as $\pm 5\%$, the polarized $\sqrt{s_{ee}} = 500$ GeV ILC can provide a better detection sensitivity of the anomalous coupling constants f_{27}:

$$-3.5 \times 10^{-2} \text{ TeV}^{-2} < f_{27}/\Lambda^2 < 3.5 \times 10^{-2} \text{ TeV}^{-2}.$$

And for $\sqrt{s_{ee}} = 1$ TeV polarized ILC, the detection sensitivity is

$$-9 \times 10^{-3} \text{ TeV}^{-2} < f_{27}/\Lambda^2 < 9 \times 10^{-3} \text{ TeV}^{-2}.$$

Both anomalous coupling f_{27} and standard model couplings appear in the same S channel Feynman diagrams, so the partial cross section is independent of the W outgoing angle and there is no kinematic differenceaaa between the anomalous coupling signal and standard model
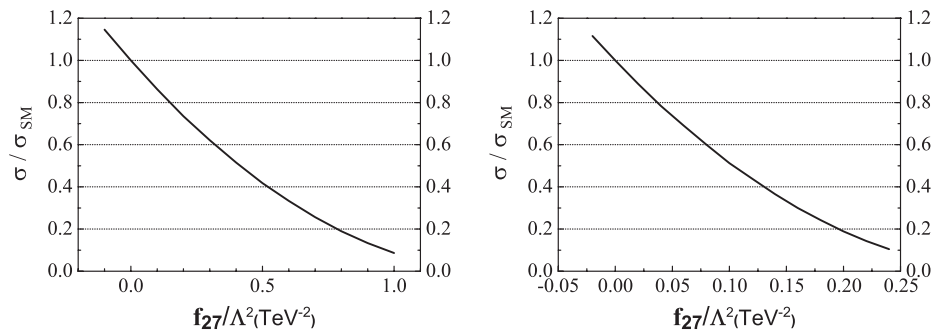

FIG. 9. The relative deviations of $e_L^+ e_R^- \rightarrow W^+W^-$ cross section at 500 GeV (left) and 1 TeV (right) ILC and caused by different anomalous coupling constants.

background. Although we cannot find any effective cuts to improve the sensitivity of the right-handed polarized electron-positron process, the ability of the polarized linear collider to detect anomalous coupling f_{27} is still improved by more than 1 order of magnitude compared to the unpolarized one.

VII. CONCLUSIONS

In this paper, we studied different electron-positron colliders' detection abilities on various effective Lagrangian coefficients of LEP2. We analyzed the anomalous couplings' effects on the $e^+e^- \rightarrow W^+W^-$ cross sections at LEP2, polarized and unpolarized ILC with 500 and 1000 GeV collision energy. We only gave the results of the single-parameter study; we simply analyzed the effect of one anomalous coupling and set all others to zero. Single-parameter study is a standard method when considering anomalous couplings' measurement. Of course, different anomalous couplings can affect the same process. While the anomalous couplings are the small deviations from SM couplings, their contributions come from the interference with SM couplings, and the interference between different anomalous couplings can be ignored. Therefore, multi-parameter contributions are almost the simple sum of single-parameter contributions when the deviations from SM are small. If there is not any deviation found at future experiments, the single-parameter study can provide a constraint on anomalous couplings. If there are some deviations found at future experiments, we should study the different kinematics distributions, different polarization scheme, or other processes to figure out what anomalous couplings cause the deviations.

Our calculations show that the higher the collision energy, the greater the ability to detect anomalous couplings. The detection sensitivity can be improved by 3–4 orders of magnitude, only when the collision energy increases by several times. This work illustrates as an example that the TeV energy linear colliders have great capability on precision measurement. The future linear colliders have multiple options, such as polarized electron-positron beam and high-energy photon colliders. Such options are helpful to measure different vertices. The scheme with right-handed polarized electrons is helpful for detecting the Z boson anomalous couplings. In this paper, we only study the single-parameter effect on the single process $e^+e^- \rightarrow W^+W^-$; any anomalous couplings beyond the detection limits can change the cross section significantly. If there are no deviations from the standard model's cross section, then all the four anomalous couplings mentioned above are within the detection bounds. However, once the future measurements observe a cross section deviation, it is difficult to determine which anomalous coupling is responsible. In this case, the study on other processes is useful, such as $e^+e^- \rightarrow ZZ(Z\gamma)$.
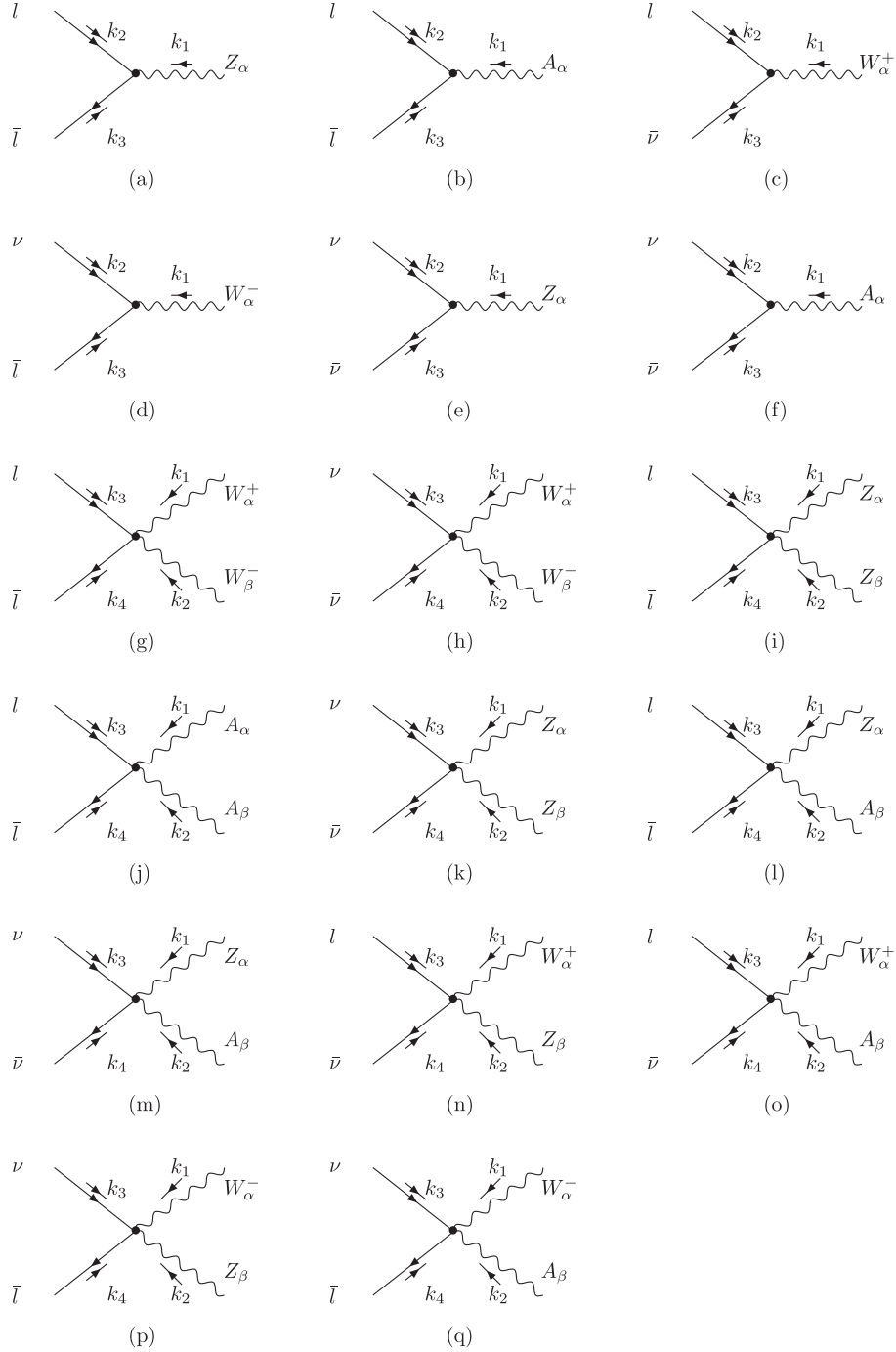
ACKNOWLEDGMENTS

APPENDIX

The Feynman rules of the dimension-6 leptonic anomalous gauge couplings:

$$(a) \quad -\frac{1}{\Lambda^2}[\not{k}_1(k_2 - k_3)^\alpha - \gamma^\alpha k_1 \cdot (k_2 - k_3)]\left(\frac{c}{2}f_7 P_L + sf_{11}P_L + sf_{13}P_R\right) + \frac{i}{\Lambda^2}[\not{k}_1 k_1^\alpha - k_1^2 \gamma^\alpha]$$
$$\times \left(\frac{c}{2}f_{24}P_L + sf_{26}P_L + sf_{27}P_R\right)$$

$$(b) \quad -\frac{1}{\Lambda^2}[\not{k}_1(k_2 - k_3)^\alpha - \gamma^\alpha k_1 \cdot (k_2 - k_3)]\left(\frac{s}{2}f_7 P_L - cf_{11}P_L - cf_{13}P_R\right) + \frac{i}{\Lambda^2}[\not{k}_1 k_1^\alpha - k_1^2 \gamma^\alpha]$$
$$\times \left(\frac{s}{2}f_{24}P_L - cf_{26}P_L - cf_{27}P_R\right)$$

$$(c) \quad \frac{1}{\Lambda^2}[\not{k}_1(k_2 - k_3)^\alpha - \gamma^\alpha k_1 \cdot (k_2 - k_3)]\left(\frac{\sqrt{2}}{2}f_7 P_L\right) + \frac{i}{\Lambda^2}[\not{k}_1 k_1^\alpha - k_1^2 \gamma^\alpha]\left(-\frac{\sqrt{2}}{2}f_{24}P_L\right)$$

(a)

(b)

(c)

(d)

(e)

(f)

(g)

(h)

(i)

(j)

(k)

(l)

(m)

(n)

(o)

(p)

(q)

$$(d) \quad \frac{1}{\Lambda^2}[\not{k}_1(k_2 - k_3)^\alpha - \gamma^\alpha k_1 \cdot (k_2 - k_3)]\left(\frac{\sqrt{2}}{2}f_7 P_L\right) + \frac{i}{\Lambda^2}[\not{k}_1 k_1^\alpha - k_1^2 \gamma^\alpha]\left(-\frac{\sqrt{2}}{2}f_{24} P_L\right)$$

$$(e) \quad -\frac{1}{\Lambda^2}[\not{k}_1(k_2 - k_3)^\alpha - \gamma^\alpha k_1 \cdot (k_2 - k_3)]\left(-\frac{c}{2}f_7 P_L + s f_{11} P_L\right) + \frac{i}{\Lambda^2}[\not{k}_1 k_1^\alpha - k_1^2 \gamma^\alpha]\left(-\frac{c}{2}f_{24} P_L + s f_{26} P_L\right)$$

$$(f) \quad -\frac{1}{\Lambda^2}[\not{k}_1(k_2-k_3)^\alpha - \gamma^\alpha k_1 \cdot (k_2-k_3)]\left(-\frac{s}{2}f_7 P_L - c f_{11} P_L\right) + \frac{i}{\Lambda^2}[\not{k}_1 k_1^\alpha - k_1^2 \gamma^\alpha]\left(-\frac{s}{2}f_{24}P_L - c f_{26}P_L\right)$$

$$(g) \quad \frac{g}{2\Lambda^2}[g^{\alpha\beta}(\not{k}_1+\not{k}_2) + \gamma^\alpha(k_4-k_1-k_3)^\beta + \gamma^\beta(k_3-k_2-k_4)^\alpha](f_7 P_L) - \frac{ig}{2\Lambda^2}[g^{\alpha\beta}(\not{k}_1-\not{k}_2)$$
$$+ \gamma^\alpha(k_4-k_1+k_3)^\beta + \gamma^\beta(-k_4+k_2-k_3)^\alpha](f_{24}P_L)$$

$$(h) \quad \frac{g}{2\Lambda^2}[g^{\alpha\beta}(\not{k}_1+\not{k}_2) + \gamma^\alpha(k_3-k_1-k_4)^\beta + \gamma^\beta(k_4-k_2-k_3)^\alpha](f_7 P_L) + \frac{ig}{2\Lambda^2}[g^{\alpha\beta}(\not{k}_1-\not{k}_2)$$
$$+ \gamma^\alpha(k_4-k_1+k_3)^\beta + \gamma^\beta(-k_4+k_2-k_3)^\alpha](f_{24}P_L)$$

$$(i) \quad -\frac{g}{\Lambda^2}[g^{\alpha\beta}(\not{k}_1+\not{k}_2) - \gamma^\alpha k_1^\beta - \gamma^\beta k_2^\alpha]\left(\frac{2s^2-1}{2}f_7 P_L + \frac{s(2s^2-1)}{c}f_{11}P_L + \frac{2s^3}{c}f_{13}P_R\right)$$

$$(j) \quad \frac{g}{\Lambda^2}[g^{\alpha\beta}(\not{k}_1+\not{k}_2) - \gamma^\alpha k_1^\beta - \gamma^\beta k_2^\alpha](s^2 f_7 P_L - 2cs f_{11}P_L - 2cs f_{13}P_R)$$

$$(k) \quad \frac{g}{\Lambda^2}[g^{\alpha\beta}(\not{k}_1+\not{k}_2) - \gamma^\alpha k_1^\beta - \gamma^\beta k_2^\alpha]\left(\frac{1}{2}f_7 P_L - \frac{s}{c}f_{11}P_L\right)$$

$$(l) \quad \frac{g}{\Lambda^2}[g^{\alpha\beta}\not{k}_1 - \gamma^\alpha k_1^\beta](cs f_7 P_L + 2s^2 f_{11}P_L) + \frac{g}{\Lambda^2}[g^{\alpha\beta}\not{k}_2 - \gamma^\beta k_2^\alpha]\left(-\frac{s(2s^2-1)}{2c}f_7 P_L + (2s^2-1)f_{11}P_L\right)$$

$$(m) \quad \frac{g}{\Lambda^2}[g^{\alpha\beta}\not{k}_2 - \gamma^\beta k_2^\alpha]\left(\frac{s}{2c}f_7 P_L + f_{11}P_L\right)$$

$$(n) \quad -\frac{g}{\Lambda^2}\frac{\sqrt{2}}{2}c[\gamma^\alpha(k_3-k_4)^\beta - \gamma^\beta(k_3-k_4)^\alpha]f_7 P_L + \frac{g}{\Lambda^2}\frac{\sqrt{2}s^2}{2c}[g^{\alpha\beta}\not{k}_1 - \gamma^\alpha k_1^\beta]f_7 P_L$$
$$-\frac{g}{\Lambda^2}\sqrt{2}s[g^{\alpha\beta}\not{k}_2 - \gamma^\beta k_2^\alpha]f_{11}P_L - \frac{ig}{\Lambda^2}\frac{\sqrt{2}c}{2}[g^{\alpha\beta}(\not{k}_1-\not{k}_2) - \gamma^\alpha(2k_1+k_2)^\beta + \gamma^\beta(k_1+2k_2)^\alpha]f_{24}P_L$$

$$(o) \quad -\frac{g}{\Lambda^2}\frac{\sqrt{2}}{2}s[\gamma^\alpha(k_3-k_4)^\beta - \gamma^\beta(k_3-k_4)^\alpha]f_7 P_L - \frac{g}{\Lambda^2}\frac{\sqrt{2}s}{2}[g^{\alpha\beta}\not{k}_1 - \gamma^\alpha k_1^\beta]f_7 P_L + \frac{g}{\Lambda^2}\sqrt{2}c[g^{\alpha\beta}\not{k}_2 - \gamma^\beta k_2^\alpha]f_{11}P_L$$
$$-\frac{ig}{\Lambda^2}\frac{\sqrt{2}s}{2}[g^{\alpha\beta}(\not{k}_1-\not{k}_2) - \gamma^\alpha(2k_1+k_2)^\beta + \gamma^\beta(k_1+2k_2)^\alpha]f_{24}P_L$$

$$(p) \quad \frac{g}{\Lambda^2}\frac{\sqrt{2}}{2}c[\gamma^\alpha(k_3-k_4)^\beta - \gamma^\beta(k_3-k_4)^\alpha]f_7 P_L + \frac{g}{\Lambda^2}\frac{\sqrt{2}s^2}{2c}[g^{\alpha\beta}\not{k}_1 - \gamma^\alpha k_1^\beta]f_7 P_L - \frac{g}{\Lambda^2}\sqrt{2}s[g^{\alpha\beta}\not{k}_2 - \gamma^\beta k_2^\alpha]f_{11}P_L$$
$$+\frac{ig}{\Lambda^2}\frac{\sqrt{2}c}{2}[g^{\alpha\beta}(\not{k}_1-\not{k}_2) - \gamma^\alpha(2k_1+k_2)^\beta + \gamma^\beta(k_1+2k_2)^\alpha]f_{24}P_L$$

$$(q) \quad \frac{g}{\Lambda^2}\frac{\sqrt{2}}{2}s[\gamma^\alpha(k_3-k_4)^\beta - \gamma^\beta(k_3-k_4)^\alpha]f_7 P_L - \frac{g}{\Lambda^2}\frac{\sqrt{2}s}{2}[g^{\alpha\beta}\not{k}_1 - \gamma^\alpha k_1^\beta]f_7 P_L + \frac{g}{\Lambda^2}\sqrt{2}c[g^{\alpha\beta}\not{k}_2 - \gamma^\beta k_2^\alpha]f_{11}P_L$$
$$+\frac{ig}{\Lambda^2}\frac{\sqrt{2}s}{2}[g^{\alpha\beta}(\not{k}_1-\not{k}_2) - \gamma^\alpha(2k_1+k_2)^\beta + \gamma^\beta(k_1+2k_2)^\alpha]f_{24}P_L$$

[1] W. Buchmuller and D. Wyler, Nucl. Phys. **B268**, 621 (1986); C. J. C. Burgess and H. J. Schnitzer, Nucl. Phys. **B228**, 464 (1983); C. N. Leung, S. T. Love, and S. Rao, Z. Phys. C **31**, 433 (1986).

[2] A. De Rujula, M. B. Gavela, P. Hernandez, and E. Masso, Nucl. Phys. **B384**, 3 (1992); K. Hagiwara, S. Ishihara, R. Szalapski, and D. Zeppenfeld, Phys. Rev. D **48**, 2182 (1993).

[3] O. J. P. Eboli, M. C. Gonzalez-Garcia, S. M. Lietti, and S. F. Novaes, Phys. Lett. B **478**, 199 (2000).

[4] F. de Campos, M. C. Ganzalez-Garcia, S. M. Lietti, S. F. Novaes, and R. Rosenfeld, Phys. Lett. B **435**, 407 (1998).

[5] D. Zeppenfeld, in *Proceedings of the APS/DPF/DPB Summer Study on the Future of Particle Physics, Snowmass, CO, 2001*, eConf C010630, P123 (2001); T. Plehn, D. Rainwater, and D. Zeppenfeld, Phys. Rev. Lett. **88**, 051801 (2002).

[6] H.-J. He, Y.-P. Kuang, C.-P. Yuan, and B. Zhang, Phys. Lett. B **554**, 64 (2003).

[7] B. Zhang, Y.-P. Kuang, H.-J. He, and C.-P. Yuan, Phys. Rev. D **67**, 114024 (2003).

[8] V. Barger, K. Cheung, A. Djouadi, B. A. Kniel, and P. M. Zerwas, Phys. Rev. D **49**, 79 (1994); M. Kramer, J. Kuhn, M. L. Stong, and P. M. Zerwas, Z. Phys. C **64**, 21 (1994); K. Hagiwara and M. Stong, Z. Phys. C **62**, 99 (1994); J. F. Gunion, T. Han, and R. Sobey, Phys. Lett. B **429**, 79

(1998); K. Hagiwara, S. Ishihara, J. Kamoshita, and B. A. Kniehl, Eur. Phys. J. C **14**, 457 (2000).

[9] V. Barger, T. Han, P. Langacker, B. McElrath, and P. M. Zerwas, Phys. Rev. D **67**, 115001 (2003).

[10] For a review on collider phenomenology, M. C. Gonzalea-Garcia, Int. J. Mod. Phys. A **14**, 3121 (1999).

[11] V. Barger, D. Marfatia, and K. Whisnant, Int. J. Mod. Phys. E **12**, 569 (2003); B. Kayser, Phys. Lett. B **592**, 1 (2004).

[12] P. Minkowski, Phys. Lett. B **67**, 421 (1977); R. N. Mohapatra and G. Senjanovic, Phys. Rev. Lett. **44**, 912 (1980); M. C. Gonzalez-Garcia and M. Maltoni, Phys. Rep. **460**, 1 (2008); R. N. Mohapatra and A. Y. Smirnov, Annu. Rev. Nucl. Part. Sci. **56**, 569 (2006).

[13] N. Arkani-Hamed, A. G. Cohen, and H. Georgi, Phys. Lett. B **513**, 232 (2001); and, for a review, see M. Perelstein, Prog. Part. Nucl. Phys. **58**, 247 (2007).

[14] C. Csaki, C. Grojean, H. Murayama, L. Pilo, and J. Terning, Phys. Rev. D **69**, 055006 (2004); C. Csaki, C. Grojean, L. Pilo, and J. Terning, Phys. Rev. Lett. **92**, 101802 (2004).

[15] J. C. Pati and A. Salam, Phys. Rev. D **10**, 275 (1974); R. N. Mohapatra and J. C. Pati, Phys. Rev. D **11**, 566 (1975); G. Senjanovic and R. N. Mohapatra, Phys. Rev. D **12**, 1502 (1975).

[16] L3 Collaboration, Phys. Lett. B **600**, 22 (2004).

[17] Particle Data Group, J. Phys. G **33**, 1 (2006).